ACS APPLIED MATERIALS & INTERFACES

www.acsami.org

Research Article

# Omnidirectional Energy Harvesting Fleeces

Chae-Lin Park,[⊥] Byeonghwa Goh,[⊥] Shi Hyeong Kim,* and Joonmyung Choi*

Cite This: *ACS Appl. Mater. Interfaces* 2023, 15, 36688−36697

Read Online

ACCESS | Metrics & More | Article Recommendations | Supporting Information

**ABSTRACT:** Underwater mechanical energy harvesters are of rising interest due to their potential for various applications, such as self-powered ocean energy harvesters, monitoring devices, and wave sensors. Pressure-responsive films and stretch-responsive fibers, which provide high electrical power in electrolytes and have simple structures that do not require packing systems, are promising as harvesters in the ocean environment. One drawback of underwater mechanical energy harvesters is that they are highly dependent on the direction of receiving external forces, which is unfavorable in environments where the direction of the supplied force is constantly changing. Here, we report spherical fleece, consisting of wool fibers and single-walled carbon nanotubes (SWCNTs), which exhibit repetitive electrical currents in all directions. No matter which direction the fleece is deformed, it changes the surface area available for ions to access SWCNTs electrochemically, causing a piezoionic phenomenon. The current per input mechanical stress of the fabricated SWCNT/wool energy harvester is up to 33.476 mA/MPa, which is the highest among underwater mechanical energy harvesters reported to date. In particular, it is suitable for low-frequency (<1 Hz) environments, making it ideal for utilizing natural forces such as wind and waves as harvesting sources. The operating mechanism in the nanoscale region of the proposed fleece harvester has been theoretically elucidated through all-atom molecular dynamics simulations.

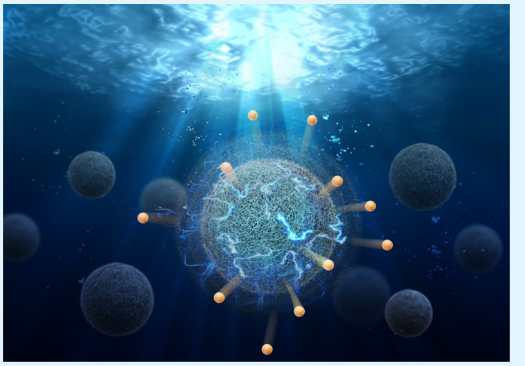

**KEYWORDS:** *underwater mechanical energy harvester, omnidirectional response, fibrous wool, carbon nanotube, molecular dynamics simulation*



## 1. INTRODUCTION

Underwater mechanical energy harvesters are promising devices that electrochemically generate electrical energy in electrolyte environments by external mechanical energy.[1−7] The device uses the ions dissolved in deionized water as the main power source, and depending on the type, it has the potential to utilize even the ions present in waterfall[2] or natural seawater.[7] The primary goal is to convert spontaneously generated mechanical energy, such as wind and ocean currents, into electrical energy. Therefore, underwater energy harvesters are likely to expand to a variety of applications, such as current monitoring devices or wave sensors for the management of marine ecosystems.

The two main types of underwater mechanical energy harvesters reported to date are liquid−solid triboelectric nanogenerators[1−3] and chemo-mechanical energy harvesters.[4−7] Both types produce electrical energy through a change in the area of an electrically or electrochemically charged surface area under mechanical force. The development direction of such energy harvesters has been focused on maximizing output power while minimizing performance drop by repeated cycles. Representative achievements include the introduction of the plied structure for increasing the maximum output to 1475 W/kg[8] and the noncontact working mode method, which maintains 96% of output even in repeated cycles of 120,000 times.[9]

However, the underwater mechanical energy harvesters developed so far have a major limitation in that they only accept external mechanical force in one direction. Since the flow of natural fluids always changes, it is reasonable to consider that the (natural) mechanical force of surrounding electrolytes in a practical operating environment cannot be controlled in all aspects of size and direction. Therefore, designing an energy harvester by limiting the orientation of the driving force seriously conflicts with the fundamentals of the device that seeks to exploit the natural mechanical energy sources found in the ocean. In other words, it is essential to design an energy harvester capable of actively coping with an external force of a broadband, low frequency, and arbitrary direction close to a naturally occurring force environment.

Motivated by the above, we propose an omnidirectional soft fleece structure composed of single-walled carbon nanotubes

Received: May 10, 2023
Accepted: June 28, 2023
Published: July 10, 2023

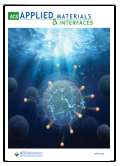

(SWCNTs) and wool composites. The proposed energy harvester is designed to target when a very small external force is supplied with a low frequency (<1 Hz) and can generate electrochemical energy by converting mechanical force in any direction. The fleece structure creates softness that responds with a large compressive strain (>50%) to small mechanical forces, resulting in the highest current per mechanical input stress compared to other underwater harvesters. The generation of electrical energy under repeated compression deformation has been demonstrated from a three-electrode system, with a measured peak current value of 150.40 $\mu$A. In addition, the nanoscale-level mechanism explaining the principle of energy generation at the SWCNT/wool composite interfaces was theoretically identified through all-atom molecular dynamics (MD) simulations.

## 2. MATERIALS AND METHODS

**2.1. Materials.** Single-walled carbon nanotube (SWCNT) powder (surface area $\geq$ 700 $m^2/g$) and isopropyl alcohol (IPA; molecular weight: 60.10 g/mol) were purchased from Sigma-Aldrich. Wool was purchased from the Ashford Store of New Zealand.

**2.2. Fabrication of the SWCNT/Wool Energy Harvester.** The SWCNT powder was dispersed in IPA by 0.05 wt % under 1 h of sonication process at a power of 117 W (sonicator: VCX 130, Vibra-Cell). Next, wool was dip-coated in the SWCNT solution for 10 min. The stability of the SWCNT/wool composites is secured by good noncovalent bonding interactions between the materials. Wool keratin contains an appropriate amount of aromatic amino acid residues, such as tyrosine (2.2%), tryptophan (0.5%), and phenylalanine (1.9%), which can provide the capability to obtain a strong $\pi-\pi$ interaction with CNTs.[10] The SWCNT/wool composites were placed in a spherical container (diameter: 35 mm) and dried overnight under a vacuum at 80 °C. By repeating this dip-coating process five times, the SWCNT/wool energy harvester of 5.3 wt % and 2.92−3.09 $kg/m^3$ was fabricated (see Figure S1 for details on the fabrication process). The prepared SWCNT/wool energy harvester samples were placed in the container and connected with Pt wire to measure the electrochemical properties (Figure S7).

**2.3. Measurement of Physical Properties of SWCNT/Wool Composites.** The state in which SWCNTs were dispersed on the wool surface was verified by field-emission scanning electron microscopy (FE-SEM, SU8010, Hitachi Co., Tokyo, Japan) images. Raman spectroscopy analyses of wool, SWCNT, and SWCNT/wool were performed using a 532 nm excitation laser (Xperam-S500, Nanobase). The data deviations due to mechanical noise were flattened to highlight important peaks. The SWCNT diameter ($d_t$) of the SWCNT/wool composite was calculated as follows

$$d_t = \frac{224}{\omega} \tag{1}$$

where $\omega$ is the wavenumber of the RBM mode peak. The stress−strain curves of the pristine wool and the SWCNT/wool composites were obtained from a texture analyzer (TA.XT Express C, Stable Micro Systems).

**2.4. Characterization of Electrochemical Energy Harvesting Behavior of SWCNT/Wool Composites.** The SWCNT/wool composites were compressed sinusoidally using a linear actuator (FE-DL100). The short-circuit current (SCC) and gravimetric capacitance change were measured using an electrochemical instrument (Zive SM6, WonA Tech). Every electrochemical measurement was conducted in a 0.1 M HCl electrolyte. The SCC was measured using the potentiostatic method, at which the external voltage was zero. All electrochemical properties in Figure 2b−e represent the average of three measurements.

The gravimetric capacitance ($C$) was calculated from the cyclic voltammetry (CV) curve as follows

$$C = \frac{A}{mk\Delta V} \tag{2}$$

where $A$ is the area of the CV curve, $m$ is the mass of the SWCNT/wool energy harvester, $k$ is the scan rate, and $\Delta V$ is the magnitude of the voltage scan range.

**2.5. Molecular Modeling to Understand the Interaction of SWCNT-Coated Wool Surfaces with Electrolytes.** To understand the interaction between the SWCNTs coated on the wool surface and the electrolyte during compressive deformation, an all-atom molecular dynamics (MD) simulation was performed. The molecular components were modeled using Materials Studio software (Dassault Systèmes, France), and the thermodynamic ensemble application in the time integration process and subsequent mechanical testing and analysis were performed using the open-source code LAMMPS (large-scale atomic/molecular massively parallel simulator; Sandia National Laboratories).[11]

The KAP8.1 (keratin-associated protein) model was used to express the molecular structure of wool in a simulation environment. The amino acid sequence of the 63-residue KAP8.1 is MLCDN FPGAV FPGCY WGSYG YPLGY SVGCG YGSTY SPVGY GFGYG YNGCG AFGYR RYSPF ALY.[12] In other words, the KAP8.1 molecule considers only the cuticle layer, which is the dominant component on the wool surface. In addition, this sequence is widely used to represent animal fur at the molecular scale.[13,14] The calculation of the interaction energy between the atoms of the peptide chain was based on the polymer consistent force field (PCFF).[15] Under a force field based on PCFF, the geometry of a single KAP8.1 chain was optimized using conjugate-gradient (CG) minimization with a 0.0002 kcal/mol/Å energy convergence criterion. The 14th, 29th, and 49th cysteines folded to form $\beta$-sheets with the same shape as that reported in previous studies,[12,16] which proves the compatibility of the force field used.

Next, an amorphous unit cell composed of 25 KAP8.1 peptide chains was generated with an initial density of 1.0 $g/cm^3$. To represent the material properties in the bulk state, periodic boundary conditions (PBCs) were applied to all $x$, $y$, and $z$ directions of the unit cell. The unit cell was equilibrated by sequentially applying an NVT ($N$: number of atoms, $V$: volume, $T$: temperature) ensemble at room temperature for 2 ns, an NPT ($P$: pressure) ensemble at room temperature, and atmospheric pressure for another 2 ns. A Nosé−Hoover thermostat and Berendsen barostat were used to control the system temperature and pressure, respectively. The density of the amorphous KAP8.1 unit cell converged to 1.13 $g/cm^3$ after thermal equilibration.

The key to molecular modeling is to construct a complex system that can track the behavior of the SWCNTs coated on the surface of KAP8.1 and the ionic layer together (Figure S9). Therefore, we first added a 16-nm-thick void layer in the z-direction to the unit cell model filled with equilibrated KAP8.1 chains. Another simulation box of 40.64 × 40.64 × 140.0 $Å^3$ size, in which 200 hydronium ($H_3O^+$) and chloride ($Cl^-$) ion pairs are randomly dispersed (density of 0.1 g/$cm^3$), was independently prepared and placed in the void area of the aforementioned unit cell. Simultaneously, eight strands of (6,5) SWCNTs (diameter of 7.6 Å) were arranged along the $y$-axis on both KAP8.1 surfaces exposed to the voids. The length of each SWCNT is 40.64 Å equal to the $y$-axis length of the unit cell, covalently bonded to each other across the PBC and thus behaves like an infinitely long nanotube. The total potential energy of the merged model was minimized using a CG gradient with a 0.001 kcal/mol/Å convergence criterion. The electrostatic effects between the atoms in the central cell and periodic images were calculated using the Ewald summation method. Subsequently, time integration was performed for 2 ns using the NVT ensemble at 300 K. During this process, the SWCNTs were fully attached to the exposed KAP8.1 surfaces. Finally, the $z$-direction length of the unit cell was reduced until the density of the area occupied by $H_3O^+$ and $Cl^-$ ions reached the experimental value of 1.07 $g/cm^3$ in a 1 M solution.[17] The unit cell contraction proceeded at a rate of 4 Å/step, and the energy of the entire system was minimized at each step using a CG gradient with a convergence criterion of 0.001


https://doi.org/10.1021/acsami.3c06644
ACS Appl. Mater. Interfaces 2023, 15, 36688−36697

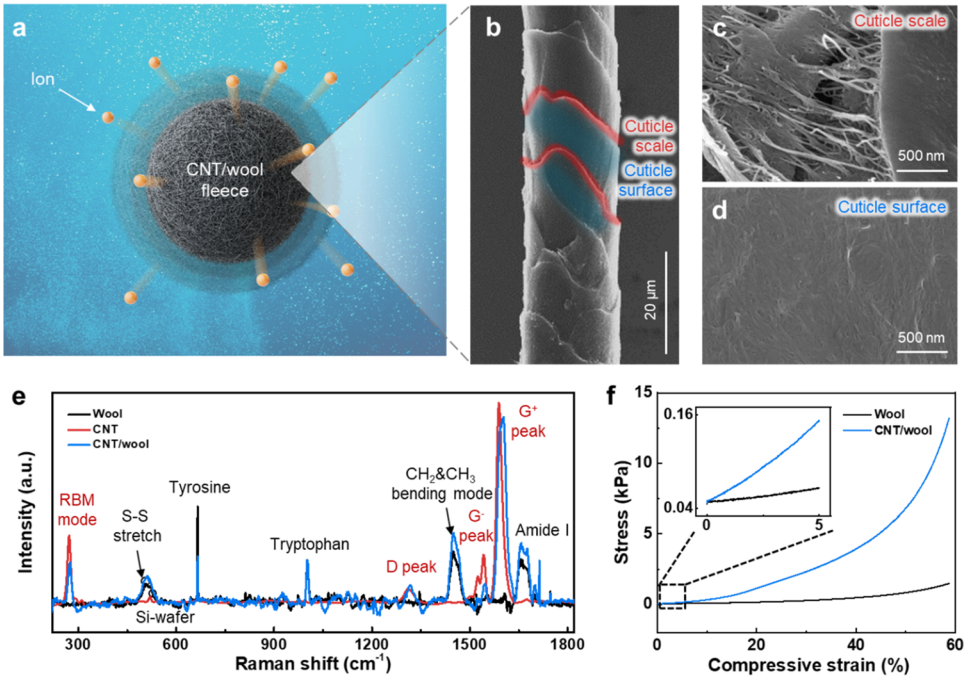


**Figure 1.** Omnidirectional SWCNT/wool energy harvester. (a) Schematic of a harvester structure that generates energy by mechanical deformation in an electrolyte. Scanning electron microscopy (SEM) images obtained for (b) single strand, (c) cuticle scale, and (d) cuticle surface domains. (e) Comparison of Raman spectroscopy analysis results of the neat wool, pristine SWCNT, and SWCNT/wool composites. (f) Stress–strain curves of the neat wool and the SWCNT/wool composites. Inset is a magnified view of the elastic deformation region (up to a strain of 5%).

kcal/mol/Å. After the ion pair density reached the desired value, the gap between the two surfaces coated with SWCNTs was reduced to 2.5 nm, and the final size of the merged cell box became 40.64 × 40.64 × 192.0 Å$^3$.

Interestingly, the surfaces composed of KAP8.1 chains show high affinity to neighboring SWCNTs. When SWCNTs were placing SWCNTs on the KAP8.1 surface, the peptide chains changed their morphology along the curvature of the SWCNT array. The shape change on the KAP8.1 surface was quantitatively plotted from molecular-scale surface roughness $R_q$ calculations (Figure S10). For the area viewed from the $x$-$y$ plane, the root-mean-square surface roughness value formed by atoms belonging to KAP8.1 is calculated as follows

$$R_q = \sqrt{\frac{L}{a}\sum_{k=1}^{n}(z_k - \bar{z})^2} \tag{3}$$

where $n$ is the number of sample data points, $L$ is the length of the cell box in the $x$-direction, and $a$ is the window size used to measure the average position of the surface atoms in the $z$-direction. The $a$ value was set at 2 Å. The analysis results of the KAP8.1 surface support two points. First, KAP8.1 readily forms physisorption on untreated SWCNTs. The $\pi$–$\pi$ stacking between the aromatic rings of tyrosine and the SWCNT surface is crucial for the formation of these strong interfacial bonds.[18] Second, the KAP8.1 chains are structurally very soft, so they do not greatly damage the array of SWCNTs during the coating process. This behavior suggests that most of the strain was applied to the wool domain when the SWCNT/wool composites were compressed to function as energy harvesters. This is related to the high deformability and durability of the SWCNT/wool composites observed in this study. The related content is covered in more detail in the analysis of the mechanical properties of each component against the compressive strain of the simulation model, which is discussed in the next section.

**2.6. Compressive Strain Simulation Inducing Contact between SWCNT-Coated Wool Surfaces.** Mechanical behavior tests were performed through uniaxial compression in the z-direction. At a strain rate of $10^7$/s, continuous compression proceeded until the z-directional cell length reached 153.6 Å.

During the compression simulation, the compressive strain in the $z$-direction ($-\varepsilon_{zz}$) was calculated using

$$-\varepsilon_{zz} = \frac{(L_{z,f} - L_{z,i})}{L_{z,f}} \tag{4}$$

where $L_{z,i}$ and $L_{z,f}$ are the $z$-direction lengths of the unit cell model before and after deformation, respectively.

Mechanical testing was performed under the NVT ensemble at 0.1 K.

During the compression simulation, the stress components caused by the changes in the internal microstructure were calculated using the virial theorem[19]

$$\boldsymbol{\sigma} = \frac{1}{\Omega}\left[-\sum_{i}^{N} m_i(\mathbf{v}_i \otimes \mathbf{v}_i) + \frac{1}{2}\sum_{i}^{N}\sum_{j\neq i}^{N}(\mathbf{r}_{ij} \otimes \mathbf{F}_{ij})\right] \tag{5}$$

where $\boldsymbol{\sigma}$ is the virial stress tensor, $\Omega$ and $N$ are the domain volume and number of atoms in the domain, $m_i$ and $\mathbf{v}_i$ are the mass and velocity of the atom $i$, and $\mathbf{F}_{ij}$ is the interaction of the relative distance ($\mathbf{r}_{ij}$) between atoms $i$ and $j$. Because the compression simulation was conducted at temperatures close to zero, the kinetic term ($m_i\mathbf{v}_i \otimes \mathbf{v}_i$) can be neglected in virial stress calculations. Because the thermal vibration of atoms due to the temperature is excluded, it is possible to evaluate the mechanical properties expressed from the pure potential energy of a given microstructure. Therefore, this mechanical testing technique is considered the best way to explicitly analyze the mechanical behavior of molecular systems and is widely used in many studies,[20,21] including our research group.[22−24] To evaluate the energetic stability between KAP8.1 and SWCNTs during deformation, the interaction energy ($E_{int}$) was calculated as follows[23,24]

$$E_{int} = \frac{E_{comp} - E_{KAP} - E_{CNT}}{A_{int}} \tag{6}$$


https://doi.org/10.1021/acsami.3c06644
ACS Appl. Mater. Interfaces 2023, 15, 36688−36697

where $A_{int}$ is the $x$-$y$ plane area of the cell box, and $E_{KAP}$, $E_{CNT}$, and $E_{comp}$ are the potential energies of the KAP8.1 chains, SWCNTs, and overall composites, respectively.

**2.7. Anisotropy of Fluidity of Ions during Compressive Strain.** The mobility of ions placed between the SWCNT-coated surfaces during the compression of the system was evaluated using mean square displacement (MSD). The MSD components in the $x$, $y$, and $z$ directions were calculated as follows

$$\mathrm{MSD}_x = \frac{1}{N}\sum_{i}^{N-1}\langle |x_i(t) - x_i(0)|^2\rangle \quad (7)$$

$$\mathrm{MSD}_y = \frac{1}{N}\sum_{i}^{N-1}\langle |y_i(t) - y_i(0)|^2\rangle \quad (8)$$

$$\mathrm{MSD}_z = \frac{1}{N}\sum_{i}^{N-1}\langle |z_i(t) - z_i(0)|^2\rangle \quad (9)$$

where the angular brackets denote the ensemble average; $x_i$ (0), $y_i$ (0), and $z_i$ (0) are the reference positions of atom $i$ in the initial configuration; and $x_i$ ($t$), $y_i$ ($t$), and $z_i$ ($t$) denote the position change at time $t$.

## 3. RESULTS AND DISCUSSION

**3.1. Preparation and Characterization of the SWCNT/Wool Energy Harvester.** The omnidirectional energy harvester was designed based on the structure in which SWCNT is coated on the surface of wool. The SWCNTs are suitable for use because of their high chemical stability in electrolytes, excellent ionic conductivity, and large specific surface area. Also, wool in the form of a fiber has high softness and flexibility, so it is easy to make a spherical structure that shows uniform mechanical deformation against any direction of force. The inherent porosity and resulting high solution absorbency of structures made from wool fibers are also advantageous for ion exchange in electrolytes. The SWCNT/wool composites were fabricated simply by the dip-coating process and have a shape in which the wool fibers coated with SWCNTs are bundled together in an irregular shape (see the Section 2.2; see Figures 1a and S1). When the harvester was subjected to an external force in any direction within the electrolyte, contact events between the coated SWCNTs were induced. In this process, the adsorbed electrolyte ions desorb and increase the potential of the system, leading to energy generation[25] (also see Figure S2 for a conceptual overview of the principles of electrical energy formation). Therefore, if a SWCNT/wool composite material with an irregular three-dimensional structure is used as an electrode, deformation in any direction can be converted into electrical energy.

Under mechanical compressive strain, contact events between SWCNTs microscopically occur, which generate electrical energy using potential changes induced by changes in the electrochemically accessible capacitance. Additionally, a larger SWCNT surface area directly exposed to the electrolyte is more advantageous for such energy harvesting.

The SWCNT/wool energy harvester was fabricated by repeating the dip-coating process, and evaluation of the electrochemical conductivity and weight indicated that a satisfactory product quality level was achieved. When pristine wool was repeatedly dip-coated with the SWCNT solution, the weight of the SWCNT/wool composite system increased and rapidly saturated (Figures S3a and S4). Accordingly, the five dip-coating cycles selected in this study were considered sufficient for SWCNTs to completely cover the wool surface. Additionally, the change in the electrochemical conductivity of the SWCNT/wool composite fibers according to the number of dip-coating cycles was confirmed using cyclic voltammetry (CV) curves (Figure S3b). Clear regions were formed in the CV curves of the composite fibers under the considered process conditions, suggesting that the material has high electrochemical conductivity properties.

Scanning electron microscopy (SEM) images of the SWCNT/wool composites clearly suggest the microstructural advantages of the proposed system. The fiber strands of the SWCNT/wool composites had alternating layers of cuticle scale and cuticle surfaces (Figure 1b). After dip-coating, the entire surface of the SWCNT/wool fibers was very rough, unlike that of the pure wool fibers (Figure S5). Interestingly, microscale porous regions were created only in cuticle scale layers (Figure 1c). The cuticle layer is the rough edges exposed on the surface and is an intrinsic structural property of wool fibers. The regions formed from the cuticle layer facilitate the hanging of SWCNTs during the dip-coating process. In contrast, the SWCNTs coated on the flat cuticle surface layer were densely packed without interstitials (Figures 1d and S5). Numerous SWCNTs are exposed from the pore surface and exposed to the outside between the cuticle scales and cuticle surface. SWCNTs in the interfacial region actively participate in ion exchange in the electrolyte and can therefore be fully utilized for energy harvesting.

The homogeneity of the fabricated SWCNT/wool composites was confirmed using Raman spectroscopy. The analysis was conducted on neat wool, pristine SWCNT, and SWCNT/wool composites (Figure 1e). The Raman spectrum of the SWCNT/wool composites contains peaks of both the neat wool and the pristine SWCNT: tyrosine (Tyr), tryptophan (Trp), amide 1, disulfide (S−S) bond stretch, $CH_2$ and $CH_3$ bending peaks of the wool,[26,27] radial breathing mode (RBM), and D, $G^-$, and $G^+$ peaks of the SWCNT.[28,29] In particular, the diameter of the SWCNTs predicted from the RBM mode peak (271.349 $cm^{-1}$) was 0.8255 nm, which did not deviate much from the original specification (0.78 nm; Sigma-Aldrich) before material compounding. The inherent nanoscale properties of SWCNTs embedded in the composites were confirmed to be well preserved without significant aggregation (see the Section 2.3). In addition, the wavenumbers of D, $G^-$ and $G^+$ peaks of the SWCNT/wool composites were blue-shifted by approximately 18 $cm^{-1}$ with compressive strain (Figure S6). It is well known that the increase in bond strength due to the reduced lattice constant under compressive stress causes an increase in the frequency and a blue shift in the peak.[30] Therefore, the present results suggest that the pressure applied to the entire system affects not only the voids between the wool fibers but also the micropore deformations between the SWCNTs.

The mechanical response of the SWCNT/wool composites to uniaxial compressive deformation was also compliant. The main advantage of pure wool fiber bundles is that they retain the elastic properties of the structure even at large deformations in excess of 50%, and the SWCNT/wool composite structure has the same properties (Figure 1f). Owing to the homogeneous coating of SWCNTs, the elastic modulus of the SWCNT/wool composite structure (2.14 kPa) was 5.6 times higher than that of the neat wool bundles (0.38 kPa). In other words, the fabricated SWCNT/wool composites significantly enhanced the effective mechanical properties without losing their structural deformability.


https://doi.org/10.1021/acsami.3c06644
ACS Appl. Mater. Interfaces 2023, 15, 36688−36697

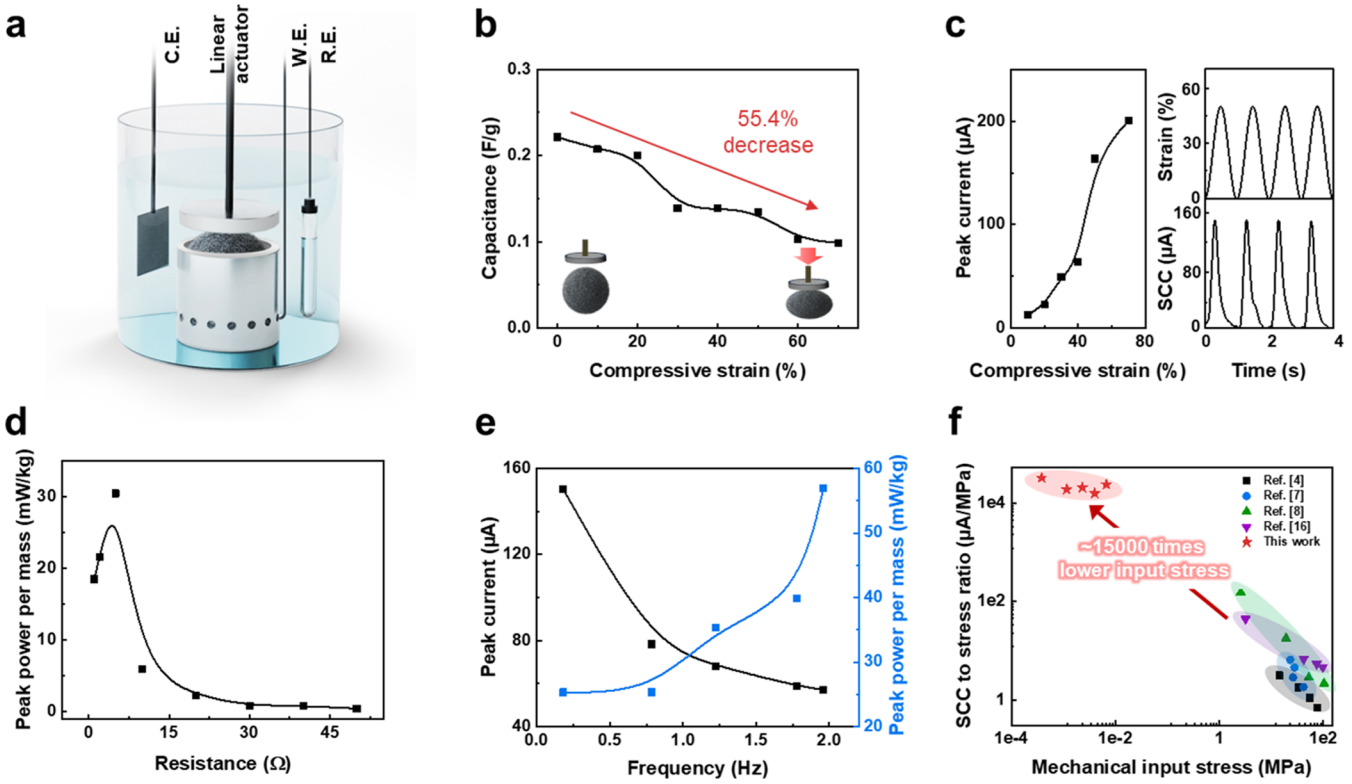


**Figure 2.** Electrochemical performance of the SWCNT/wool energy harvester in a 0.1 M HCl electrolyte. (a) Experimental setup of a three-electrode system for characterization of fabricated samples in an electrolyte. (b) Change in capacitance of the SWCNT/wool energy harvester by compressive strain. The capacitance measurements were made under cyclic voltammetry scans at 50 mV/s. (c) Peak short-circuit current (SCC) measured during increasing compressive strain. The right panel shows the repetitively applied compressive strain as a sinusoidal wave at 1 Hz in the SWCNT/wool energy harvester (top) and the resulting SCC response profile (bottom). (d) Peak power per mass induced by the load resistance for the SWCNT/wool energy harvester when compressed to 50% at 1 Hz. (e) Peak values of SCC and power per mass of the SWCNT/wool energy harvester as a function of compressive strain frequency. (f) Ratio of SCC to mechanical input stress of the SWCNT/wool energy harvester compared to previous chemo-mechanical energy harvesters.

**3.2. Electrochemical Performance of the SWCNT/Wool Energy Harvester.** The practical energy-harvesting performance of the fabricated SWCNT/wool composite structures was evaluated. A three-electrode system was used to quantitatively measure the electrochemical properties of the SWCNT/wool energy harvester (Figure 2a). The three-electrode system consisted of a working electrode (W.E.) with a SWCNT/wool harvester, a counter electrode (CE) with a Pt mesh/CNT buckypaper, and a reference electrode (RE) with Ag/AgCl attached. The W.E. was prepared by inserting SWCNT/wool composites at a density of 3.09 kg/m$^3$ into a spherical cage (Figure S7). A linear actuator was installed above the cylinder barrel to measure the changes in the system properties when the internal composite structures were compressed.

The capacitance of the energy harvester as an electrode is the primary factor that determines the electrochemical performance of a system. As compressive strain up to 70% was progressively applied, the capacitance exhibited by the SWCNT/wool energy harvester decreased linearly by approximately 55.4% from 0.22 to 0.098 F/g (Figures 2b and S8). The capacitance change clearly shows that the SWCNT/wool composites can be used as an electrode in electrochemical energy harvesters.

The performance of SWCNT/wool energy harvesters was characterized (Figure 2c). The short-circuit current (SCC) change measured at the W.E responded almost instantaneously to the cyclic compressive strain and did not degrade under repeated operation. If the compressive strain increases, the peak SCC increases linearly and the maximum peak SCC was obtained as 200.46 $\mu$A at 70% of compressive strain. The SWCNT/wool energy harvester generated an electrical peak power of 30 mW/kg at 5 Ω (Figure 2d), and such a low matching impedance indicates high energy transfer efficiency.[22] The electrochemical performance also depends on the frequency of sinusoidal compressive strain (Figure 2e). The condition for the SWCNT/wool energy harvester to achieve the highest peak current of 150.40 $\mu$A is at a very low frequency of 0.18 Hz. As the frequency increases, the impedance decreases and the peak power increases to 57 mW/kg within the observation range.

It is worth noting that the present findings on SWCNT/wool energy harvesters are particularly suitable for harnessing the continuously and widely varying mechanical energy generated by the ocean. Because of the inherent softness of the fleece structure, the mechanical input stress required to drive the SWCNT/wool energy harvester is approximately 15,000 times lower than that of other chemo-mechanical energy harvesters. As a result, the proposed SWCNT/wool energy harvester achieved the highest SCC to input stress ratio (> $10^2$) among chemo-mechanical energy harvesters reported so far[4,7,8,31] (Figure 2f). Such extremely sensitive responsiveness to mechanical loads is an important factor in ensuring the


https://doi.org/10.1021/acsami.3c06644
ACS Appl. Mater. Interfaces 2023, 15, 36688−36697

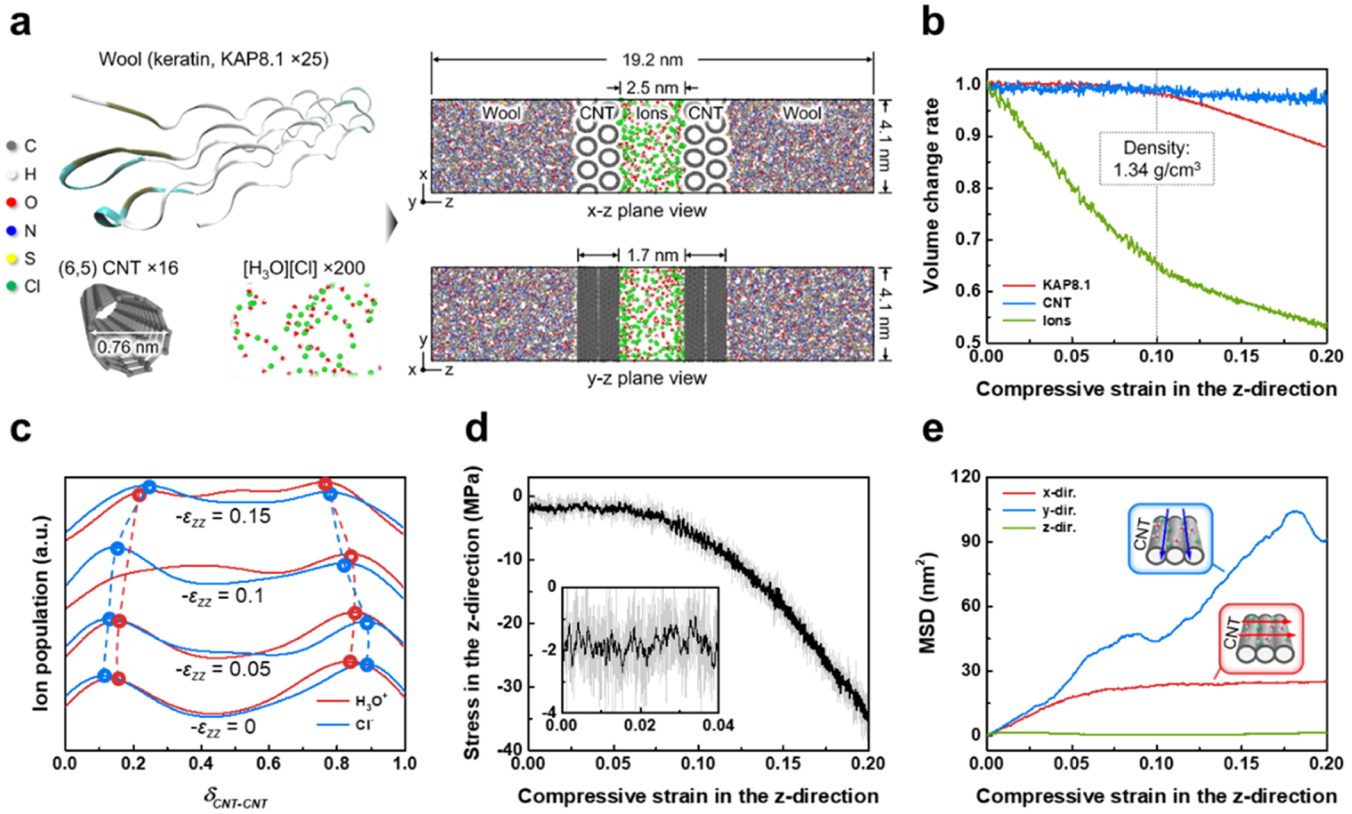


**Figure 3.** Comprehension of the electrolyte kinetics on the surface of the SWCNT/wool composites through the MD simulation. (a) Computational model describing the microstructure in which SWCNTs are placed on the wool surface. The molecular structures of the constituents considered in the simulation model, KAP8.1, (6,5) SWCNT, and $H_3O^+$ and $Cl^-$ ions, are shown in the left panel. The thermal equilibrium state of the microstructure in which SWCNT/wool and electrolyte coexist is presented in the right panel (top: front view, bottom: side view). The folded corners and the straight $\beta$-sheets of the KAP8.1 structure are colored blue and white, respectively. A ribbon diagram representation of KAP8.1 was drawn using the STRIDE algorithm[32] implemented in VMD software.[33] Other all-atom configurations were presented using OVITO software.[34] (b) Volume change of KAP8.1 chains, SWCNTs, and ions during compressive strain. The effective volume occupied by the atoms was defined according to the Connolly algorithm[35] with a probe radius of 2.5 Å. (c) Population density changes in the z-direction of $Cl^-$ and $H_3O^+$ ions. All distributions are plotted in the area where the relative distance between two SWCNT-coated surfaces (denoted by $\delta_{CNT\text{-}CNT}$) is normalized to 1. The circular symbols connected by the dotted lines highlight shifts in the peak values of the ion distribution during compression. (d) Virial stress component exerted on the ions in the $z$-direction. The scattered lines show raw data obtained every $10^{-7}$ engineering strain. The bold lines are the moving average results for 30 consecutive data points. (e) MSD profiles of the ions during compression. The insets represent the direction of ionic motion versus the arrangement in which the SWCNTs are placed.

operation of the harvester even with small external forces, maximizing its operability in real environments.

**3.3. Molecular-Scale Simulation of Energy Harvesting Mechanism of SWCNTs/Wool Composites.** So far, it has been experimentally demonstrated that a wool fleece coated with SWCNTs can function as an energy harvester. This suggests that the macroscopic compressive strain of the structure effectively induced the flow of ions around the SWCNTs in the nanoscale region. Therefore, it is necessary to explain the principle by which SWCNT/wool composites can exhibit meaningful electrochemical performance and high durability. In this regard, all atomic molecular dynamics (MD) simulations were performed to clearly understand the mechanical properties of the SWCNT/wool composites and the behavior of the electrolyte during operation.

The molecular model for the MD simulation consists of an electrolyte in which $H_3O^+$ and $Cl^-$ form ion pairs, and the keratin-associated protein 8.1 gene (KAP8.1) surfaces coated with SWCNTs are adjacent to it (Figure 3a; also refer to Section 2.5 and Figure S9 for details of the model preparation). In the coated area, the KAP8.1 chains were gently wrapped around the SWCNTs without destroying their cylindrical shape (Figure S10).[26,36] When the system received an external mechanical load, the mechanical response of each component of the composites (see the Section 2.6) and the mobility characteristics of the electrolyte (see the Section 2.7) were simultaneously evaluated.

As forcible compressive strain was applied, each component of the system experienced different volume changes (Figure S11). The volume of the ion pair in the fluid state decreased most rapidly, and at a compression rate of 10% or more, KAP8.1 also compresses together (Figure 3b). On the other hand, the SWCNT layer preserves its original shape between KAP8.1 and ions. The structure of the coated SWCNT layer was not distorted, even when the density of the entire molecular-scale system reached 1.34 g/cm$^3$. As a result, ion pairs do not pass through the coated surface composed of SWCNT arrays (Figure S12). This shows that the van der Waals interactions formed by the SWCNTs within a bundle were sufficiently robust to prevent neighboring diffusing atoms from penetrating into the surface. The ion pairs trapped in the microscopic region where the SWCNT bundles contact each other do not disintegrate the coating layer during compressive deformation but rather generate repulsive forces between the


https://doi.org/10.1021/acsami.3c06644
ACS Appl. Mater. Interfaces 2023, 15, 36688−36697

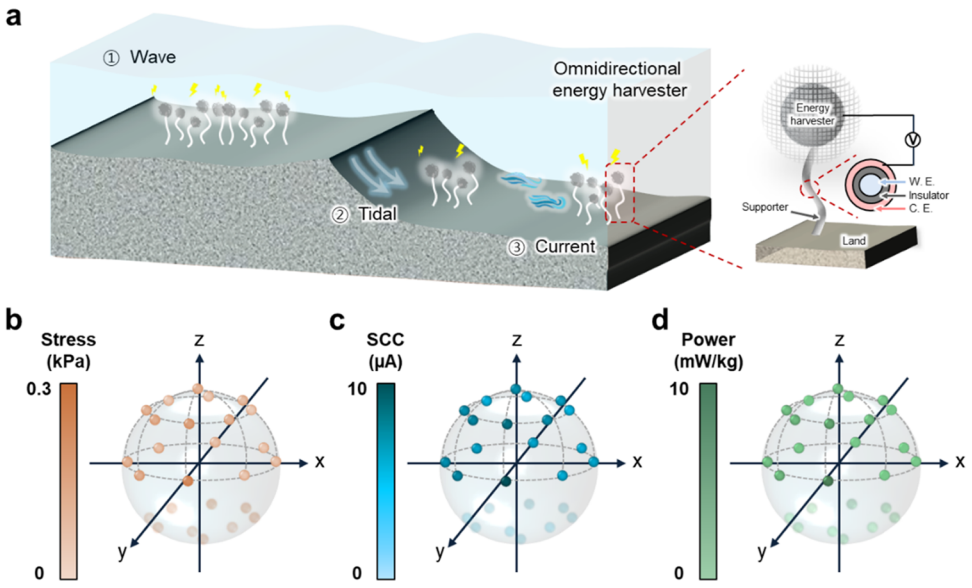


**Figure 4.** Demonstration of omnidirectional response of the omnidirectional energy harvester. (a) Illustration of the omnidirectional energy harvester application in ocean environments. The unit system is composed of two separate components, namely, the SWCNT/wool energy receiver and a support. The support can be designed as a multilayered coaxial structure consisting of a conductive electrode, insulator, and counter electrode connected to a SWCNT/wool energy harvester. (b) Compressive stress applied to the SWCNT/wool fleece at various locations in three-dimensional space and the resulting (c) peak SCC and (d) peak power. The color brightness is assigned according to the size of the data measured at each location.

ions. Macroscopically, the repulsive force becomes the driving force that causes ions to escape the cuticle layer and leak.

The existence of such a repulsive force was also confirmed by the distribution of ion pairs around the SWCNT array during compression (Figure 3c). In the absence of mechanical strain, $Cl^-$ was located closer to the SWCNT surface than $H_3O^+$. It is typical for $Cl^-$ ions to be trapped closer to the SWCNT surface because they are heavier, less mobile, and have stronger physicochemical bonds with carbon atoms than $H_3O^+$ ions.[37,38] However, the tendency rapidly collapsed when the compressive strain exceeded 0.1, and the polarization characteristics disappeared. The stress component experienced by the ions in the axial direction during compressive deformation also suggests the same implication. In the undeformed state, the ions were polarized and adsorbed on the SWCNT array, forming an intrinsic repulsive stress of about −2 MPa (Figure 3d). As compression proceeds, the repulsive stress applied to the ions maintains an equilibrium and then increases rapidly. When the compressive strain of the entire system reached 0.2, the value reaches approximately −35 MPa. This value is sufficiently large to escape ions from the physisorption formed by the SWCNT array covering the cuticle layer. Meanwhile, the SWCNT and KAP8.1 chains receive three times more stress than ions because they withstand both the repulsive force from ions and the pressure from external deformation (Figure S13). In particular, SWCNT prevented ions from being immersed in the matrix beyond the SWCNT coating area while maintaining a constant interaction force with KAP8.1 (Figure S14).

**3.4. Omnidirectionality of System Performance.** Finally, the mobility of ions owing to the repulsive force shows a high correlation with the arrangement of the SWCNT array. The mean square displacement (MSD) profile analysis results for each direction show that the ions move along the surface of the SWCNT array using the repulsive force supplied by compression (Figure 3e). However, little movement in the z-direction away from the SWCNT array was observed. In particular, the mobility in the y-direction parallel to the SWCNT array increased noticeably after the compressibility of the system reached a level that collapsed the ion-polarization layer. In other words, as the repulsion between ions intensified, not only did the noncovalent bonding force form with the carbon atoms of SWCNTs but also the structural shape of the SWCNT array had a significant effect on the ion flow.

In real marine environments, the direction of ocean power sources, including surface waves, tides, and currents, is constantly changing, and thus, how well the above energy harvesting mechanisms will work is unpredictable (Figure 4a). In other words, to demonstrate realistic energy harvesting performance, independent evaluation of omnidirectional responses to external forces in all directions is required. Therefore, the dependence of the energy-harvesting properties of the SWCNT/wool fleece on numerous external force directions was investigated. A spherical SWCNT/wool fleece was prepared, and 17 checkpoints were designated according to the latitude and longitude of the surface (Figure 4b–d). The checkpoints were specified only for the upper hemisphere region, and all compressive forces were applied normally to the surface. The compressive stress was applied in a range from 0 to 0.3 kPa, and the peak SCC and peak power that occurred at each stress were recorded at the corresponding location. For all measured points, the peak SCC and peak power were observed from 1.3 to 9.5 $\mu$A and from 1.2 to 9.7 mW/kg, respectively, which clearly proves the omnidirectional nature of the proposed SWCNT/wool fleece.

The proposed fleece structure can be operated at any location when packaged with the electrolyte and electrode, further expanding its applicability. In this respect, an all-in-one electrochemical system containing the WE, CE, and electrolyte was developed, and its performance was qualitatively evaluated. The packaging was carried out with a rabbit-shaped rubber balloon so that the force applied to the WE did not damage the


https://doi.org/10.1021/acsami.3c06644
ACS Appl. Mater. Interfaces 2023, 15, 36688−36697

CE (Figure S15). Each time the fleece located on the working electrode was repeatedly pressed with bare hands, an SCC change was detected. In particular, when the test was conducted by dividing the method of gripping by hand into three stages (nudging, pressing, and grasping), it was confirmed that the size of the change in SCC was measured at a classifiable level (Figure S16).

## 4. CONCLUSIONS

Although this test was conducted in a naive and non-quantitative environment, the results demonstrate the high potential of the proposed structure as a novel mechanical sensor. For example, this system can be developed as a cognitive developmental training tool for infants, who emit a signal when a blow comes from an arbitrary direction. When used in the form embedded in the ball, it is highly likely to be used as a training aid and for precise technical analysis in various sports games. In the environmental industry, the system can be applied as a detector that observes the blowing direction and size of winds and ocean currents in real time in three dimensions, which cannot be observed with the naked eye.

In the design of a soft energy harvester, removing constraints on the direction of the external force is as important as increasing the absolute performance or efficiency of the system. The fleece structure proposed in this study utilizes the unique capacitance characteristics of SWCNTs but is not constrained by the direction of compression deformation; therefore, its usability is greatly increased compared to existing harvesters. Owing to the structure in which the fibers are loosely entangled, the system can withstand a large amount of deformation, and the material constituting each fiber strand is lightweight and flexible. Experiments have proven that the maximum SCC values of the proposed fleece energy harvester are 6.71 mV and 200.46 $\mu$A, respectively, under 70% compressive strain. In particular, the fleece structure has high energy harvesting performance at low frequencies (<1 Hz); therefore, it can be directly used in natural environments, such as waves, wind, and tides.

The findings of this study are the first to demonstrate the potential of fleece structures as next-generation soft energy harvesters. The biggest advantage is the removal of constraints on the direction of the external force, and it is believed that further improvements in performance and efficiency will continue to be possible. From the perspective of manufacturing composite materials, maximizing the cuticle interfaces, in which the direct contact of SWCNTs with the external electrolyte actually occurs, can increase the energy density of the system. The electrolyte considered in this study was an ion pair of $H_3O^+$ and $Cl^-$, which is one of the most primitive conditions. However, it is believed that there are suitable types of ion pairs and concentration conditions that exhibit better performance, depending on the effective properties of the SWCNT/wool composites and the usage environment. It is also important to design the mechanical behavior characteristics at the interface of the microstructure. The size of the SWCNTs being coated, the coating density of SWCNTs in the cuticle interfacial layer, and the effective strain experienced by the interface region under operating conditions are also expected to govern the absolute performance of the system. Finally, designing an appropriate shape for efficient energy harvesting in an asymmetrical situation where external force with local directivity is supplied is also a major concern.

## ■ ASSOCIATED CONTENT

### Data Availability Statement

The data used to produce the results of this study will be provided upon reasonable request

### Supporting Information

The Supporting Information is available free of charge at https://pubs.acs.org/doi/10.1021/acsami.3c06644.

Schematic of the fabrication process of SWCNT/wool composite fiber strands; schematic diagram of the principle of current and voltage formation between the SWCNT and wool fibers; weight saturation process of the SWCNT/wool composite system; color changes of the SWCNT/wool fibers; SEM images of the pure wool and SWCNT/wool fibers; Raman spectra; SWCNT/wool composite container; CV curves of the SWCNT/wool composites; preparation of an all-atom model; molecular-scale roughness before and after SWCNTs was coated on the surface of KAP8.1 chains; snapshots of the layered molecular structure during unidirectional compression; distribution of ions lying between both CNT surfaces; axial stress components; robustness of interfaces between SWCNTs and KAP8.1 chains; rabbit-shaped balloon energy harvester; empirical evaluation of energy harvesting through an all-in-one system (PDF)

## ■ AUTHOR INFORMATION


### Corresponding Authors

**Shi Hyeong Kim** − *HYU-KITECH Joint Department, Hanyang University, Seoul 04763, Republic of Korea; Department of Advanced Textile R&D, Korea Institute of Industrial Technology, Ansan-si 15588 Gyeonggi-do, Republic of Korea*; Email: shk@kitech.re.kr

**Joonmyung Choi** − *HYU-KITECH Joint Department, Hanyang University, Seoul 04763, Republic of Korea; Department of Mechanical Design and Engineering, Hanyang University, Seoul 04763, Republic of Korea; Department of Mechanical Engineering, BK21 FOUR ERICA-ACE Center, Hanyang University, Ansan-si 15588 Gyeonggi-do, Republic of Korea*; orcid.org/0000-0003-3673-8069; Email: joonchoi@hanyang.ac.kr

### Authors

**Chae-Lin Park** − *HYU-KITECH Joint Department, Hanyang University, Seoul 04763, Republic of Korea; Department of Advanced Textile R&D, Korea Institute of Industrial Technology, Ansan-si 15588 Gyeonggi-do, Republic of Korea*

**Byeonghwa Goh** − *Department of Mechanical Design and Engineering, Hanyang University, Seoul 04763, Republic of Korea; Department of Mechanical Engineering, BK21 FOUR ERICA-ACE Center, Hanyang University, Ansan-si 15588 Gyeonggi-do, Republic of Korea*

Complete contact information is available at: https://pubs.acs.org/10.1021/acsami.3c06644


### Author Contributions

$^{\perp}$C.-L. Park and B. Goh contributed equally and should be considered co-first authors. C.-L.P. performed the fabrication, experiments, measurements, and data management, and interpreted the results. B.G. performed the modeling, simulations, and data management and interpreted the results. S.H.K. and J.C. supervised this study. All authors contributed to writing and reviewing the manuscript



https://doi.org/10.1021/acsami.3c06644
ACS Appl. Mater. Interfaces 2023, 15, 36688−36697

## Notes

The authors declare no competing financial interest.

## ■ ACKNOWLEDGMENTS

This work was supported by the Korea Institute of Industrial Technology (KITECH JE230016). Also, this work was supported by the National Research Foundation of Korea (NRF) grant funded by the Korea government (MSIT) (No. RS-2023-00210865).

## ■ REFERENCES

(1) Zhang, X.; Yu, M.; Ma, Z.; Ouyang, H.; Zou, Y.; Zhang, S. L.; Niu, H.; Pan, X.; Xu, M.; Li, Z.; Wang, Z. L. Self-Powered Distributed Water Level Sensors Based on Liquid−Solid Triboelectric Nanogenerators for Ship Draft Detecting. *Adv. Funct. Mater.* **2019**, *29*, No. 1900327.

(2) Zhao, X. J.; Zhu, G.; Fan, Y. J.; Li, H. Y.; Wang, Z. L. Triboelectric Charging at the Nanostructured Solid/Liquid Interface for Area-Scalable Wave Energy Conversion and Its Use in Corrosion Protection. *ACS Nano* **2015**, *9*, 7671−7677.

(3) Zhu, G.; Su, Y.; Bai, P.; Chen, J.; Jing, Q.; Wang, W.; Wang, Z. L. Harvesting Water Wave Energy by Asymmetric Screening of Electrostatic Charges on a Nanostructured Hydrophobic Thin-Film Surface. *ACS Nano* **2014**, *8*, 6031−6037.

(4) Kim, S. H.; Haines, C. S.; Li, N.; Kim, K. J.; Mun, T. J.; Choi, C.; Di, J.; Oh, Y. J.; Oviedo, J. P.; Bykova, J.; Fang, S.; Jiang, N.; Liu, N.; Wang, R.; Kumar, P.; Qiao, R.; Priya, S.; Cho, K.; Kim, M.; Lucas, M. S.; Drummy, L. F.; Maruyama, B.; Lee, D. Y.; Lepró, X.; Gao, E.; Albarq, D.; Ovalle-Robles, R.; Kim, S. J.; Baughman, R. H. Harvesting Electrical Energy from Carbon Nanotube Yarn Twist. *Science* **2017**, *357*, 773−778.

(5) Wang, Z.; Mun, T. J.; Machado, F. M.; Moon, J. H.; Fang, S.; Aliev, A. E.; Zhang, M.; Cai, W.; Mu, J.; Hyeon, J. S.; Park, J. W.; Conlin, P.; Cho, K.; Gao, E.; Wan, G.; Huynh, C.; Zakhidov, A. A.; Kim, S. J.; Baughman, R. H. More Powerful Twistron Carbon Nanotube Yarn Mechanical Energy Harvesters. *Adv. Mater.* **2022**, *34*, No. 2201826.

(6) Mun, T. J.; Kim, S. H.; Park, J. W.; Moon, J. H.; Jang, Y.; Huynh, C.; Baughman, R. H.; Kim, S. J. Wearable Energy Generating and Storing Textile Based on Carbon Nanotube Yarns. *Adv. Funct. Mater.* **2020**, *30*, No. 2000411.

(7) Oh, S.; Kim, K. J.; Goh, B.; Park, C.-L.; Lee, G. D.; Shin, S.; Lim, S.; Kim, E. S.; Yoon, K. R.; Choi, C.; Kim, H.; Suh, D.; Choi, J.; Kim, S. H. Chemo-Mechanical Energy Harvesters with Enhanced Intrinsic Electrochemical Capacitance in Carbon Nanotube Yarns. *Adv. Sci.* **2022**, *9*, No. 2203767.

(8) Zhang, M.; Cai, W.; Wang, Z.; Fang, S.; Zhang, R.; Lu, H.; Aliev, A. E.; Zakhidov, A. A.; Huynh, C.; Gao, E.; Oh, J.; Moon, J. H.; Park, J. W.; Kim, S. J.; Baughman, R. H. Mechanical Energy Harvesters with Tensile Efficiency of 17.4% and Torsional Efficiency of 22.4% Based on Homochirally Plied Carbon Nanotube Yarns. *Nat. Energy* **2023**, *8*, 203−213.

(9) Cao, B.; Wang, P.; Rui, P.; Wei, X.; Wang, Z.; Yang, Y.; Tu, X.; Chen, C.; Wang, Z.; Yang, Z.; Jiang, T.; Cheng, J.; Wang, Z. L. Broadband and Output-Controllable Triboelectric Nanogenerator Enabled by Coupling Swing-Rotation Switching Mechanism with Potential Energy Storage/Release Strategy for Low-Frequency Mechanical Energy Harvesting. *Adv. Energy Mater.* **2022**, *12*, No. 2202627.

(10) Zhu, S.; Zhou, Q.; Yi, J.; Xu, Y.; Fan, C.; Lin, C.; Wu, J.; Lin, Y. Using Wool Keratin as a Structural Biomaterial and Natural Mediator to Fabricate Biocompatible and Robust Bioelectronic Platforms. *Adv. Sci.* **2023**, *10*, No. 2207400.

(11) Thompson, A. P.; Aktulga, H. M.; Berger, R.; Bolintineanu, D. S.; Brown, W. M.; Crozier, P. S.; in't Veld, P. J.; Kohlmeyer, A.; Moore, S. G.; Nguyen, T. D.; Shan, R.; Stevens, M. J.; Tranchida, J.; Trott, C.; Plimpton, S. J. LAMMPS - A Flexible Simulation Tool for Particle-based Materials Modeling at the Atomic, Meso, and Continuum Scales. *Comput. Phys. Commun.* **2022**, *271*, No. 108171.

(12) Singh, R. S.; Palmer, J. C.; Pudney, P. D. A.; Paul, P. K. C.; Johannessen, C.; Debenedetti, P. G.; Raut, J.; Lee, K.; Noro, M.; Tiemessen, D. Molecular Modeling and Structural Characterization of a High Glycine−tyrosine Hair Keratin Associated Protein. *Phys. Chem. Chem. Phys.* **2017**, *19*, 8575−8583.

(13) Matsunaga, R.; Abe, R.; Ishii, D.; Watanabe, S.; Kiyoshi, M.; Nöcker, B.; Tsuchiya, M.; Tsumoto, K. Bidirectional Binding Property of High Glycine−tyrosine Keratin-associated Protein Contributes to the Mechanical Strength and Shape of Hair. *J. Struct. Biol.* **2013**, *183*, 484−494.

(14) Jin, M.; Wang, L.; Li, S.; Xing, M. X.; Zhang, X. Characterization and Expression Analysis of KAP7.1, KAP8.2 Gene in Liaoning New-breeding Cashmere Goat Hair Follicle. *Mol. Biol. Rep.* **2011**, *38*, 3023−3028.

(15) Sun, H.; Mumby, S. J.; Maple, J. R.; Hagler, A. T. An ab Initio CFF93 All-Atom Force Field for Polycarbonates. *J. Am. Chem. Soc.* **1994**, *116*, 2978−2987.

(16) Pentelute, B. L.; Gates, Z. P.; Tereshko, V.; Dashnau, J. L.; Vanderkooi, J. M.; Kossiakoff, A. A.; Kent, S. B. X-ray Structure of Snow Flea Antifreeze Protein Determined by Racemic Crystallization of Synthetic Protein Enantiomers. *J. Am. Chem. Soc.* **2008**, *130*, 9695−9701.

(17) Ishiyama, T.; Morita, A. Molecular Dynamics Analysis of Interfacial Structures and Sum Frequency Generation Spectra of Aqueous Hydrogen Halide Solutions. *J. Phys. Chem. A* **2007**, *111*, 9277−9285.

(18) Yang, Z.; Wang, Z.; Tian, X.; Xiu, P.; Zhou, R. Amino Acid Analogues Bind to Carbon Nanotube via $\pi$-$\pi$ Interactions: Comparison of Molecular Mechanical and Quantum Mechanical Calculations. *J. Chem. Phys.* **2012**, *136*, No. 025103.

(19) Heyes, D. M. Pressure Tensor of Partial-charge and Point-dipole Lattices with Bulk and Surface Geometries. *Phys. Rev. B* **1994**, *49*, 755−764.

(20) Subramaniyan, A. K.; Sun, C. T. Continuum Interpretation of Virial Stress in Molecular Simulations. *Int. J. Solid Struct.* **2008**, *45*, 4340−4346.

(21) Choi, J.; Shin, H.; Yang, S.; Cho, M. The Influence of Nanoparticle Size on the Mechanical Properties of Polymer Nanocomposites and the Associated Interphase Region: A Multiscale Approach. *Compos. Struct.* **2015**, *119*, 365−376.

(22) Goh, B.; Choi, J. A Spatial Upscaling Method for Describing the Three-body Potential of a Diamond Lattice Structure. *Appl. Math. Model.* **2022**, *108*, 502−511.

(23) Kim, M.; Goh, B.; Kim, J.; Kim, K.-S.; Choi, J. Regeneration of Interfacial Bonding Force of Waste Carbon Fibers by Light: Process Demonstration and Atomic Level Analysis. *iScience* **2022**, *25*, No. 105367.

(24) Lim, J.; Goh, B.; Qu, W.; Kim, Y.; Choi, J.; Hong, S. Adhesive-free Bonding of PI/PDMS Interface by Site-selective Photothermal Reactions. *Appl. Surf. Sci.* **2022**, *571*, No. 151123.

(25) McCarty, L. S.; Whitesides, G. M. Electrostatic Charging Due to Separation of Ions at Interfaces: Contact Electrification of Ionic Electrets. *Angew. Chem., Int. Ed.* **2008**, *47*, 2188−2207.

(26) Church, J. S.; Corino, G. L.; Woodhead, A. L. The Analysis of Merino Wool Cuticle and Cortical Cells by Fourier Transform Raman Spectroscopy. *Biopolymers* **1997**, *42*, 7−17.

(27) Notayi, M.; Hunter, L.; Engelbrecht, J. A.; Botha, A. F.; Minnaar, E. G.; Lee, M. E.; Erasmus, R. The Application of Raman Spectroscopic Ratiometric Analysis for Distinguishing between Wool and Mohair. *J. Nat. Fibers* **2022**, *19*, 11536−11546.

(28) Yan, X.; Itoh, T.; Kitahama, Y.; Suzuki, T.; Sato, H.; Miyake, T.; Ozaki, Y. A Raman Spectroscopy Study on Single-Wall Carbon Nanotube/Polystyrene Nanocomposites: Mechanical Compression Transferred from the Polymer to Single-Wall Carbon Nanotubes. *J. Phys. Chem. C* **2012**, *116*, 17897−17903.

(29) Heller, D. A.; Barone, P. W.; Swanson, J. P.; Mayrhofer, R. M.; Strano, M. S. Using Raman Spectroscopy to Elucidate the Aggregation



https://doi.org/10.1021/acsami.3c06644
ACS Appl. Mater. Interfaces 2023, 15, 36688−36697

State of Single-Walled Carbon Nanotubes. *J. Phys. Chem. B* **2004**, *108*, 6905−6909.
(30) Hui, Y. Y.; Liu, X.; Jie, W.; Chan, N. Y.; Hao, J.; Hsu, Y.-T.; Li, L.-J.; Guo, W.; Lau, S. P. Exceptional Tunability of Band Energy in a Compressively Strained Trilayer MoS2 Sheet. *ACS Nano* **2013**, *7*, 7126−7131.
(31) Wang, Z.; Mun, T. J.; Mun, T. J.; Machado, F. M.; Moon, J. H.; Fang, S.; Aliev, A. E.; Zhang, M.; Cai, W.; Mu, J.; Hyeon, J. S.; Park, J. W.; Conlin, P.; Cho, K.; Gao, E.; Wan, G.; Huynh, C.; Zakhidov, A. A.; Kim, S. J.; Baughman, R. H. More Powerful Twistron Carbon Nanotube Yarn Mechanical Energy Harvesters. *Adv. Mater.* **2022**, *34*, No. 2201826.
(32) Frishman, D.; Argos, P. Knowledge-based Protein Secondary Structure Assignment. *Proteins* **1995**, *23*, 566−579.
(33) Humphrey, W.; Dalke, A.; Schulten, K. VMD: Visual Molecular Dynamics. *J. Mol. Graphics* **1996**, *14*, 33−38.
(34) Stukowski, A. Visualization and Analysis of Atomistic Simulation Data with OVITO−the Open Visualization Tool. *Model. Simul. Mater. Sci. Eng.* **2009**, *18*, No. 015012.
(35) Connolly, M. L. Solvent-Accessible Surfaces of Proteins and Nucleic Acids. *Science* **1983**, *221*, 709−713.
(36) Goh, B.; Kim, K. J.; Park, C.-L.; Kim, E. S.; Kim, S. H.; Choi, J. In-plane Thermal Conductivity of Multi-walled Carbon Nanotube Yarns under Mechanical Loading. *Carbon* **2021**, *184*, 452−462.
(37) Miyamoto, Y.; Zhang, H.; Rubio, A. First-Principles Simulations of Chemical Reactions in an HCl Molecule Embedded inside a C or BN Nanotube Induced by Ultrafast Laser Pulses. *Phys. Rev. Lett.* **2010**, *105*, No. 248301.
(38) Xu, B.; Chen, X. Liquid Flow-induced Energy Harvesting in Carbon Nanotubes: A Molecular Dynamics Study. *Phys. Chem. Chem. Phys.* **2013**, *15*, 1164−1168.


https://doi.org/10.1021/acsami.3c06644
*ACS Appl. Mater. Interfaces* 2023, 15, 36688−36697